Metrol. Meas. Syst., Vol. 30 (2023) No. 3, pp. 549–561
DOI: 10.24425/mms.2023.146415

PAN POLSKA AKADEMIA NAUK

METROLOGY AND MEASUREMENT SYSTEMS
Index 330930, ISSN 0860-8229
www.metrology.wat.edu.pl

M&MS

AN ALTERNATING CURRENT CALIBRATION METHOD FOR HELMHOLTZ COIL CONSTANT BASED ON ORTHOGONAL CALCULATION PRINCIPLE

Kuankuan Zhang[1,2)], Mingxing Cao[1)], Jian He[1)], Wenjie Gong[1)], Yunhua Huang[2)]

1) Magnetic Materials Measurement Laboratory, National Institute of Metrology, Beijing 100029, China (*zhangkk369@163.com*, *caomx@nim.ac.cn*, ✉ *hejian@nim.ac.cn*, *wjgong@nim.ac.cn*)
2) University of Science and Technology Beijing, Beijing 100083, China (*huangyh@mater.ustb.edu.cn*)

Abstract

The Helmholtz coil constant (k_h) is a crucial standard in magnetic moment measurement devices for permanent magnet materials. To overcome the problem of low accuracy of the direct-current (DC) calibration method, this study used a constant sinusoidal current in the Helmholtz coil and measured the induced voltage of the detection coil with known coil turns and coil area. Subsequently, the k_h was calculated. The noise signal deduction rate in the induction voltage of the detection coil was greater than 99%, its influence on the induction voltage is less than 0.005%, and the repeatability of the calibration results is 0.003% (1δ). The results reveal that the alternating current (AC) method and *orthogonal calculation* (OC) can accurately measure the valid values of the voltage signal under the influence of the spatial stray field during the calibration of k_h.

Keywords: Helmholtz coils constant; alternating current method; induction voltage; orthogonal calculations.

1. Introduction

The Helmholtz coil is a key device for the magnetic moment metrology of permanent magnet materials [1–4]. It is a pair of circular coils connected in series in the same direction to generate a uniform magnetic field of low intensity and large range [5–10]. Generally, the ratio of magnetic flux to k_h determines the basic standard of magnetic moment measurement of permanent-magnet materials.

The theoretical formula for k_h is the induced current flowing through the coil divided by the magnetic field strength at the centre of the coil. The induced current can be measured precisely. Therefore, we must use a magnetic field sensor to accurately measure the magnetic field strength at the centre of the coil to calculate k_h [11]. However, the conventional method of k_h calibration involves passing a constant DC current through a Helmholtz coil, measuring the magnetic field at the centre of the coil with a magnetometer, and calculating the coil constant from the measured values of the magnetic field and current [12]. However, the disadvantage of such methods is that the

Article history: received December 28, 2022; revised April 24, 2023; accepted April 30, 2023; available online September 15, 2023.

magnetic field generated by the Helmholtz coil is approximately 10–100 Gs at the allowed current. The geomagnetic field, stray field, and zero point of the measuring instrument have a significant impact on the measurement results [13–17], and the uncertainty of the coil constant calibration results is approximately 0.3% [18]. Therefore, instead of directly measuring the magnetic-field strength at the centre of the coil, the coil constant can be calculated indirectly by measuring the induced voltage at the centre of the coil.

Orthogonal computation has been used to model low-dimensional dynamic applications in engineering and science [19–23]. It is accomplished by establishing the corresponding basis functions via orthogonal decomposition of the experiments or data of the physical system, followed by analysing the effects of the basic functions on the physical system and making the corresponding compensations to improve the entire physical model.

In this study, we propose a calibration method for the k_h test and measurement system based on the AC method and develop the corresponding calibration method. The calibration of k_h is achieved by passing an AC through the Helmholtz coil and measuring the AC coil constant at a certain frequency. The valid values of the voltage signal are accurately measured under the interference of external environments, such as the spatial stray field. Also the error factors affecting the experimental results are analysed.

2. Calibration methods and principles of calibration stand

2.1. Calibration method

The calibration method involves placing a detection coil with a known number of turns and area in the centre of the Helmholtz coil and then passing a constant sinusoidal current through the Helmholtz coil to calculate the Helmholtz coil constant by measuring the induced voltage, sinusoidal current, and frequency. The calculation formulas are expressed as follows:

$$U_{\text{rms}} = 2\pi f \cdot NS \cdot \mu_0 \cdot k_h \cdot I_{\text{rms}}\,, \tag{1}$$

$$k_h = \frac{U_{\text{rms}}}{2\pi f \cdot NS \cdot \mu_0 \cdot I_{\text{rms}}}\,, \tag{2}$$

where U_{rms} denotes the valid value of the induced voltage of the detection coil, f denotes the signal source frequency, N indicates the number of detection coil turns, S symbolizes the area of the detection coil, μ_0 symbolizes the vacuum magnetic permeability, and I_{rms} indicates the valid value of the excitation current.

The direct measurement of the valid value of the induced voltage causes a large error in the calibration results because the induced voltage of the detection coil contains both useful and stray field signals. Therefore, the stray signals in the induced voltage should be removed by using the quadrature principle to calculate the active and reactive powers of the induced voltage; thus, the valid value of the induced voltage can be accurately determined. The calculation formulas are expressed as follows:

$$P = U_{\text{rms}} \cdot I_{\text{rms}} \cos\varphi = \frac{1}{n}\sum_{i=1}^{n} U_i \cdot I_i\,, \tag{3}$$

$$Q = U_{\text{rms}} \cdot I_{\text{rms}} \sin\varphi = \frac{1}{n}\sum_{i=1}^{n} U_i \cdot I_{i+\frac{n}{4}}\,, \tag{4}$$

Metrol. Meas. Syst., Vol. 30 (2023), No. 3, pp. 549–561
DOI: 10.24425/mms.2023.146415

$$U_{\text{rms}} = \frac{\sqrt{P^2 + Q^2}}{I_{\text{rms}}}, \tag{5}$$

where P denotes active power, Q symbolizes the reactive power, φ indicates the phase angle, U_i indicates the voltage at i point, I_i indicates the current at i point, $I_{i+n/4}$ is the current at the $i+n/4$ point. Active power was calculated for each point on the real curve using a digital power meter. However, reactive power cannot be calculated in this manner because the instrument is limited in its scope. As illustrated in Fig. 1, the cycle points are enhanced as the frequency decreases, collected at multiples of five. Thus, the sampling points in a cycle cannot be exactly divided into four, and the shift cannot be accurately controlled at 90°. Thus, P and Q cannot be calculated using the orthogonal principle.

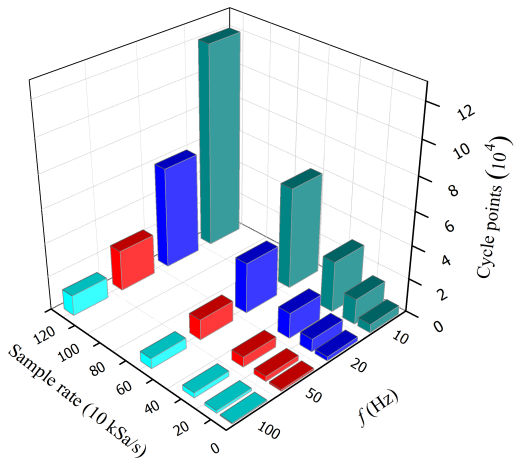

Fig. 1. Corresponding relation between the sampling rate and sampling points per period.

A novel method to solve this problem is to translate the collected current points into two different phases. Considering a 50 Hz, 50.505 kSa/s sampling rate as an example, the measurement principle is as follows:

1. Move 100 points of the collected current data points and multiply them point-by-point with the voltage points to obtain P';
2. Move 300 points of the collected current data points and multiply them point-by-point with the voltage points again to obtain Q'. In other words, there is a phase difference of 200 points between them (the phase difference can be set arbitrarily). The calculation formulas are expressed as follows:

$$P' = \frac{1}{n}\sum_{i=0}^{n} U_i I_{i+100} = UI\cos\varphi, \tag{6}$$

$$Q' = \frac{1}{n}\sum_{i=0}^{n} U_i I_{i+300} = UI\cos\left(\varphi + \varphi_{200}\right). \tag{7}$$

According to the trigonometric sum and difference formula, (7) is expanded and expressed as:

$$Q' = UI\cos(\varphi + \varphi_{200}) = UI\cos\varphi\cos\varphi_{200} - UI\sin\varphi\sin\varphi_{200}, \tag{8}$$

$$\frac{Q' - \cos\varphi_{200} P'}{\sin\varphi_{200}} = -UI\sin\varphi, \tag{9}$$

where $\sin\varphi_{200}$ and $\cos\varphi_{200}$ are constants. Next both sides of (6) and (9), respectively are squared, and then the sum added to obtain (10).

$$P'^2 + \left(\frac{Q' - \cos\varphi_{200} P'}{\sin\varphi_{200}}\right)^2 = U^2 I^2. \tag{10}$$

In addition, the discrete method of the current calculation formula can be expressed as follows.

$$I = \sqrt{\frac{1}{n}\sum_{i=0}^{n} I_i^2}. \tag{11}$$

From (10) and (11), the valid value of the induced voltage can be accurately obtained to cancel the external interfering signals to the maximum extent possible. This indicates that accurate measurement of low-voltage signals can be achieved using the OC. In other words, the induction voltage obtained from the measurement is consistent with the frequency of the excitation current signal, whereas interference signals, such as external radio signals of different frequencies and industrial frequency power signals are filtered out. Table 1 lists the induction voltage measurement results after adopting the orthogonal principle at different phase angles. The deviation of the calculation results at different phase angles was ±0.001%, which illustrates the accuracy and effectiveness of the algorithm.

Table 1. Voltage measurement results of orthogonal method at different phase angles.

Initial angle (°)	Phase difference (°)	Voltage measurement results (V)
23.76	23.76	0.150135
23.76	35.64	0.150137
23.76	47.52	0.150137
23.76	59.40	0.150137
23.76	71.28	0.150138
23.76	83.16	0.150138
23.76	95.05	0.150138
47.52	23.76	0.150137
47.52	47.52	0.150137
71.28	47.52	0.150137
83.16	47.52	0.150137

2.2. Principles of calibration stand

The k_h calibration stand, as illustrated in Fig. 2, consists of a Helmholtz coil, arbitrary waveform generator, power amplifier, and digital power meter. The power amplifier amplifies this signal to a suitable intensity to provide Helmholtz coil AC excitation. Under the excitation of an alternating magnetic field, the detection coil placed in the central uniform area of the Helmholtz coil generates an induced voltage signal which is sent to the voltage sensor end of the digital power meter for accurate voltage measurement.

Metrol. Meas. Syst., Vol. 30 (2023), No. 3, pp. 549–561
DOI: 10.24425/mms.2023.146415

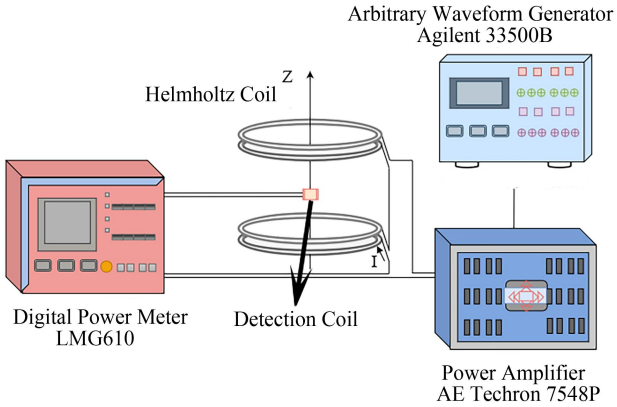

Fig. 2. Schematic of the Helmholtz coil constant calibration stand.

The arbitrary waveform generator used is an Agilent 33500B, which provides a signal source for a high-stability power amplifier with a total harmonic distortion of 0.04%. The power meter used is an LMG610 which measures the induced voltage of a small coil and the excitation current with high accuracy. The LMG610 power meter has a U_{sensor} mode which can directly measure the induced voltage of the small coil. The U_{sensor} input voltage range is 0–4 V, and the maximum allowable error is ±(0.01% reading +0.02% full scale). The high-stability power amplifier used is an AE Techron 7548P, which provides a stable current for calibrating the Helmholtz coil. The maximum output power is 3300 W RMS, and the output frequency is DC – 200 kHz, with a DC drift of ±200 μV. Prior to the measurement, these devices were calibrated and their uncertainty was analysed to meet the requirements of measurement accuracy.

As illustrated in Figs. 3a and 3b, the design of the Helmholtz coils follows the criteria of identical shape, coaxial placement, equal number of turns, equal resistance, same magnitude and direction of the load current, coil spacing equal to the radius, and parallelism between the two coils.

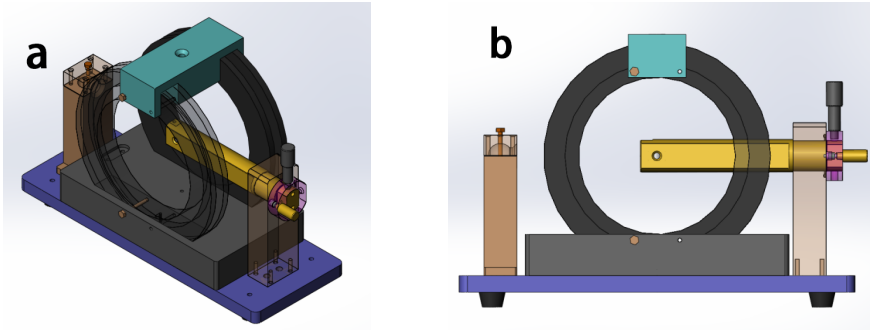

Fig. 3. Design of R120 Helmholtz coil (a) axonometric drawing, (b) frontal view.

When calibrating the Helmholtz coil using an induction coil, it is necessary to not only ensure that they are parallel to each other through mechanical design, but also to find the position of the maximum induced voltage signal through fine adjustment of the induction coil. This is necessary to ensure that the induction coil and the Helmholtz coil are parallel to each other and achieve the

lowest calibration uncertainty. As shown in Fig. 4, we have designed an angle adjustment function for the induction coil which is mounted on a fixed shaft. The left side of the fixed shaft is spherical and connected to the fixed bracket and the clamping cover, respectively. During calibration, the fixed shaft is finely rotated around its centre point, and when the position of the maximum induced voltage signal of the induction coil is found, the clamping cover screw can be tightened. At this point, the induction coil and the Helmholtz coil are parallel to each other. Fig. 5 shows a physical image of the Helmholtz coil.

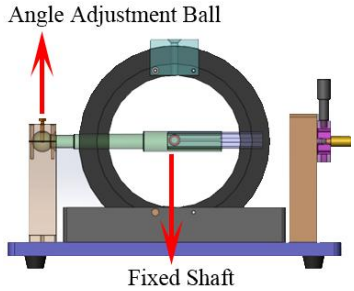

Fig. 4. Schematic diagram of gimbal-adjusted spatial positioning of the induction coil.

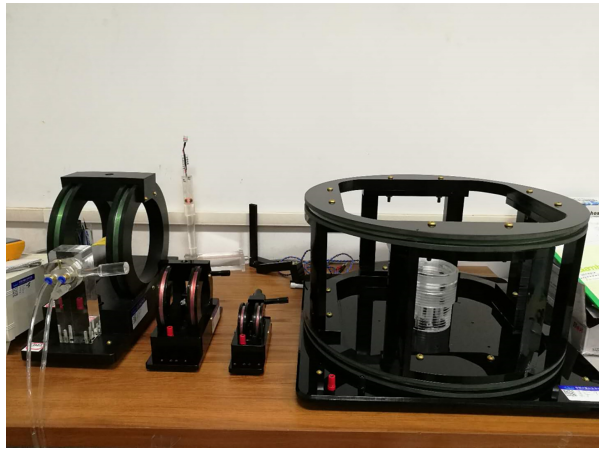

Fig. 5. Physical image of the Helmholtz coil.

3. Helmholtz coil calibration test

3.1. Elimination of voltage background noise signal with the orthogonal calculation method

Figure 6 illustrates the elimination of the background noise signal of the induction voltage in the detection coil after using the quadrature calculation method at different frequencies.

Based on the measurement results, except for the induction voltage noise signal in the detection coil at 40 Hz, which reaches 3.3 mV, the induction voltage noise signal in the detection coil at other frequencies is approximately 1.8 mV. This is because during the experiment with a 40 Hz excitation current, short-term interference signals suddenly occurred around it, such as nearby

Metrol. Meas. Syst., Vol. 30 (2023), No. 3, pp. 549–561
DOI: 10.24425/mms.2023.146415

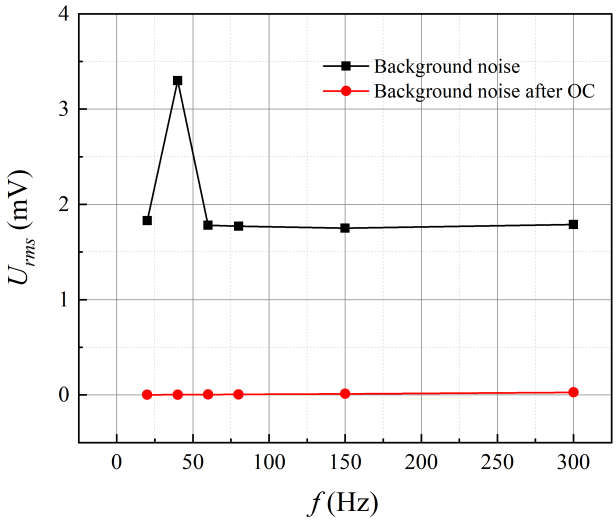

Fig. 6. Elimination of background noise of voltage measurement with the OC method at different frequencies. The illustration shows the consistency of elimination of background noise of voltage measurement with the OC method at the same frequency (60 Hz).

instruments suddenly starting up or phones ringing. These signals vary in duration, amplitude, and occurrence time, and are not specific to the 40 Hz frequency, and may also occur at other frequencies in the same experiment. Upon using the OC method, the background noise signal was reduced to approximately 0.008 mV and the deduction rate of the background noise reached 99.6%. At different frequencies, the background noise of the induction voltage of the detection coil obtained using the OC method is significantly reduced compared to the untreated background noise; in other words, most of the useless interference signals are effectively deducted, and the influence of the background noise on the voltage measurement is reduced to within 0.005% following the use of the OC method.

Table 2 lists the elimination of the background signal of the induction voltage of the detection coil using the quadrature principle at the same frequency. The background noise of the induction voltage signal of the detection coil was measured six times at 60 Hz, and the background noise

Table 2. Consistency of the background noise elimination of voltage measurement with the orthogonal calculation method at 60 Hz.

Frequency / Hz	**Background noise / mV**	**Orthogonal calculation background noise / mV**	**Background noise deduction rate**	**Calibration Voltage / mV**	**Effect of background noise on voltage measurement after orthogonal computation**
60	1.78	0.004	99.78%	173.3	0.0023%
60	1.76	0.004	99.77%	173.3	0.0023%
60	1.76	0.003	99.83%	173.3	0.0017%
60	1.74	0.003	99.83%	173.3	0.0017%
60	1.75	0.004	99.77%	173.3	0.0023%
60	1.76	0.004	99.77%	173.3	0.0023%

was measured after using the OC method. It is evident that the background noise of the induction voltage obtained after the detection coil at 60 Hz reaches 1.76 mV on average. On average, the background noise of the induction voltage obtained after the OC is reduced to 0.0037 mV, and the background noise deduction rate of the induction voltage exceeds 99.7%. The influence of the background noise on the induced voltage after using the OC is reduced to less than 0.003%. The measurement results show that by using the OC method, the background noise can be reduced to an extremely low level, and the measurement repeatability remains almost consistent.

3.2. Variation of the Helmholtz coil constant with frequency

Table 3 illustrates the relationship between the variation in k_h and frequency where the vertical coordinate data are normalized. As shown in the table, k_h increases rapidly with frequency when the frequency is higher than 1000 Hz, whereas within 1000 Hz, the change in k_h with increasing frequency is less than 0.1%, and in the range of 5–100 Hz, the change is less than ±0.02%. This range of variation is equivalent to the voltage measurement accuracy of a digital power meter. Hence, by reducing the signal frequency of the sinusoidal AC to below 100 Hz during the calibration of k_h, the coil constant is considered not to change with the increase in frequency.

Table 3. Trends of Helmholtz coil constants with frequency.

Frequency / Hz	5	10	20	30	40	50	60	80	100	200
Normalization	1.00002	1.00002	1	1	1	1	1	0.99992	0.99985	0.9998
Frequency / Hz	300	400	600	800	1000	1300	1500	2000	2500	3000
Normalization	0.99978	0.99976	0.99982	0.99999	1	1.0019	1.0028	1.00595	1.00721	1.0149

3.3. Repeatability of Helmholtz coil constant measurements

Figure 7 presents the results of the k_h repeatability measurements after using the OC method. Ten measurements were performed on the Helmholtz coil using the same probe coil, after which the probe coil was removed from the calibrated Helmholtz coil and returned. The results of the

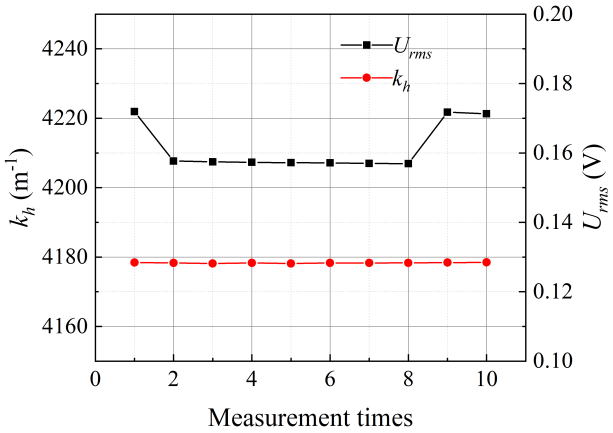

Fig. 7. Repeated measurement results of the coil constants of Helmholtz coils.

Metrol. Meas. Syst., Vol. 30 (2023), No. 3, pp. 549–561
DOI: 10.24425/mms.2023.146415

ten measurements reveal that the average value of the induced voltage of the probe coil is 0.16 V, and the measurement repeatability of k_h is 0.003% (expressed as the standard deviation).

4. Uncertainty analysis of Helmholtz coil constant AC method calibration

4.1. Uncertainty introduced by measurement repeatability (u_A)

As a Class A uncertainty, u_A covers random differences in different testers, concave coil placement, etc. As previously mentioned, the k_h measurement repeatability was 0.003% (1δ), and the distribution law was normal distribution.

4.2. Uncertainty introduced by the influence of the instrumentation used for calibration on the measurement results (u_B)

As a type B uncertainty, u_B covers the influence of the uncertainty introduced by instrumental measurement and the distribution law was normal distribution. The power meter was set to the U_{sensor} mode with a frequency of 60 Hz, and then the 0.17 V point was calibrated. Following the calibration, the absolute value of the average voltage measurement error was 0.02% and the calibration uncertainty was 0.02%. The input impedance of the power meter was 100 kΩ, and the resistance of the detection coil was 350 Ω; thus, the voltage division effect of the detection coil resistance is approximately 0.35%. The frequency of the port input signal was measured using a power meter with an accuracy of ±50 ppm, which is a normal distribution. The power meter was set to the current mode with a frequency of 60 Hz, and then the 0.4 A point was calibrated. Following the calibration, the absolute value of the average current measurement error was 0.025% and the calibration uncertainty was 0.01%.

As mentioned above, the measurement uncertainty caused by the background noise is 0.005%, and within the range of 5–100 Hz, the coil constant is stable within ±0.02%, which is equivalent to the voltage measurement accuracy of the power meter. Ambient temperature also affected the winding area of the Helmholtz coil. The expansion coefficient of copper wire is 16.56×10^{-6}°C, and the expansion coefficient of Plexiglass is 60×10^{-6}°C. Owing to the uncertainty of temperature measurement, which is 0.3°C, the change in Helmholtz coil diameter is 0.002%.

4.3. Synthetic uncertainty analysis

The uncertainty analysis of the Helmholtz coil constant calibration according to the JJF 1059-2012 Measurement uncertainty assessment and representation is listed in Table 4 and the aforementioned uncertainty components are summarized in the table. The table covers the uncertainty sources, index of uncertainty sources, input uncertainty values, distribution type, divisor, sensitivity factor, standard uncertainty (1σ), and effective degrees of freedom (v_{eff}). The relative extended uncertainty of the Helmholtz coil constant calibration was calculated to be 1% ($k = 2$) using (12).

$$\left[\frac{u_x(y)}{y}\right]^2 = \sum_{i=1}^{N}\left[p_i \frac{u(x_i)}{x_i}\right]^2, \tag{12}$$

where y denotes the output estimate, $u_x(y)$ indicates the synthetic standard uncertainty of y, p denotes the probability, x_i indicates the input estimate, and $u(x_i)$ represents the synthetic standard uncertainty of x.

Table 4. Summary of k_h calibration uncertainty.

Uncertainty sources	Value ±(%)	Divisor	c_1	u_1 ±(%)	v_{eff}
Measurement accuracy on the U_{sensor} side of the digital power meter	0.027	2	1	0.0135	inf.
Detecting the effect of voltage division of coil resistance	0.002	2	1	0.0010	inf.
Frequency measurement accuracy of digital power meters	0.005	2	1	0.0025	inf.
I_{rms} measurement accuracy of digital power meters	0.027	2	1	0.0135	inf.
Effect of background noise	0.005	2	1	0.0025	inf.
Consistency of measurement results at different frequencies	0.020	2	1	0.0100	inf.
Magnetic field stability of Helmholtz coils	0.020	2	1	0.0100	inf.
Effect of Helmholtz coil uniformity zone on calibration	0.070	2	1	0.0350	inf.
Detection of the perpendicularity of the coil plane to the Helmholtz coil axis	0.015	2	1	0.0075	inf.
Effect of ambient temperature on calibration	0.002	2	2	0.0020	inf.
Measurement repeatability	0.003	1	1	0.0030	11
Standard Synthetic Uncertainty				0.0472	673863
Extended Uncertainty	1	$k = 2$		0.0944	

5. Conclusions

Considering the key role of the Helmholtz coil in permanent magnetic moment measurement and the defects of DC method calibration, this paper proposes an AC calibration method for the Helmholtz coil constant, designs, and establishes a AC method calibration stand and calibration scheme for the Helmholtz coil. Moreover, a traceability system is established, the sources of uncertainty of the calibration system are analysed, and the relative extended uncertainty of the calibration results is evaluated.

1. Using the orthogonal calculation principle to calibrate k_h at different signal frequencies, the deduction rate of the external noise signal reached 99.6%, and its impact on the induction voltage of the detection coil was reduced to within 0.005%. The calibration k_h at a fixed frequency of 60 Hz, the deduction rate of the background noise signal surpassed 99.7%, and its impact on the induction voltage of the detection coil was reduced to 0.003%.
2. When the signal frequency was between 5 and 100 Hz, the calibration result of k_h in the AC state did not vary by more than 0.02%.
3. Upon using the AC method and orthogonal principle to calibrate k_h, the repeatability of the calibration results was 0.003% (1δ), and the relative extended uncertainty was 1% ($k = 2$).

Acknowledgements

This work was supported by the State Administration for Market Regulation of China (No. ANL1912).

References

[1] Zhao, Z. N., Lin, J., Zhang, J., Yu, Y., Yuan, B., Fan, C. C., & Liu, J. (2018). Liquid metal enabled flexible electronic system for eye movement tracking. *IEEE Sensors Journal*, *18*(6), 2592–2598. https://doi.org/10.1109/JSEN.2018.2796121

Metrol. Meas. Syst., Vol. 30 (2023), No. 3, pp. 549–561
DOI: 10.24425/mms.2023.146415

[2] Li, Z., & Dixon, S. (2016). A closed-loop operation to improve GMR sensor accuracy. *IEEE Sensors Journal*, *16*(15), 6003–6007. https://doi.org/10.1109/JSEN.2016.2580742

[3] Lapucci, T., Troiano, L., Carobbi, C., & Capineri, L. (2021). Soft and Hard Iron Compensation for the Compasses of an Operational Towed Hydrophone Array without Sensor Motion by a Helmholtz Coil. *Sensors*, *21*(23), 8104. https://doi.org/10.3390/s21238104

[4] Nelson, I., Gardner, L., Carlson, K., & Naleway, S. E. (2019). Freeze casting of iron oxide subject to a tri-axial nested Helmholtz-coils driven uniform magnetic field for tailored porous scaffolds. *Acta Materialia*, 173, 106–116. https://doi.org/10.1016/j.actamat.2019.05.003

[5] Markoulakis, E., Vanderelli, T., & Frantzeskakis, L. (2022). Real time display with the ferrolens of homogeneous magnetic fields. *Journal of Magnetism and Magnetic Materials*, 541, 168576. https://doi.org/10.1016/j.jmmm.2021.168576

[6] Pang, H., Duan, L., Quan, W., Wang, J., Wu, W., Fan, W., & Liu, F. (2020). Design of highly uniform three dimensional spherical magnetic field coils for atomic sensors. *IEEE Sensors Journal*, *20*(19), 11229–11236. https://doi.org/10.1109/JSEN.2020.2997800

[7] Fernquist, J. R., Fu, H. C., & Naleway, S. E. (2022). Improved structural and mechanical performance of iron oxide scaffolds freeze cast under oscillating magnetic fields. *Ceramics International*, *48*(1), 15034–15042. https://doi.org/10.1016/j.ceramint.2022.02.032

[8] Jiang, J., Yang, L., & Zhang, L. (2021). Closed-loop control of a Helmholtz coil system for accurate actuation of magnetic microrobot swarms. *IEEE Robotics and Automation Letters*, *6*(2), 827–834. https://doi.org/10.1109/LRA.2021.3052394

[9] Alamgir, A. K. M., Fang, J., Gu, C., & Han, Z. (2005). Square Helmholtz coil with homogeneous field for magnetic measurement of longer HTS tapes. *Physica C: Superconductivity*, *424*(1-2), 17–24. https://doi.org/10.1016/j.physc.2005.04.019

[10] Alvarez, A. F. R., Franco-Mejia, E., & Pinedo-Jaramillo, C. R. (2012, November). Study and analysis of magnetic field homogeneity of square and circular Helmholtz coil pairs: A Taylor series approximation. In *2012 VI Andean Region International Conference* (pp. 77–80). IEEE. https://doi.org/10.1109/Andescon.2012.27

[11] Watakabe, R., Tanaka, M., Takahashi, Y., Fujiwara, K., Ishihara, Y., & Azuma, D. (2016). Study on standard measurement method of magnetic property of Fe-based amorphous strip — Round Robin test results. *IEEE Transactions on Magnetics*, *52*(5), 1–4. https://doi.org/10.1109/TMAG.2016.2518209

[12] Ishii, M., & Suzuki, M. (2020, August). Impedance of Helmholtz Coil to Generate Standard AC Magnetic Field in High Frequency. *In 2020 Conference on Precision Electromagnetic Measurements* (CPEM) (pp. 1–2). IEEE. https://doi.org/10.1109/CPEM49742.2020.9191906

[13] Yue, L., Cheng, D., Wang, Y., Wang, M., & Zhao, J. (2021). A comprehensive calibration method for non-orthogonal error and scale factor error of triaxial Helmholtz coil. *Review of Scientific Instruments*, *92*(8), 085105. https://doi.org/10.1063/5.0049784

[14] Mu, Y., Wang, C., Zhang, X., & Xie, W. (2018). A novel calibration method for magnetometer array in nonuniform background field. *IEEE Transactions on Instrumentation and Measurement*, *68*(10), 3677–3685. https://doi.org/10.1109/TIM.2018.2880079

[15] Liu, Z., Zhang, Q., Pan, M., Shan, Q., Geng, Y., Guan, F., ... & Tian, W. (2016). Distortion magnetic field compensation of geomagnetic vector measurement system using a 3-D Helmholtz coil. *IEEE Geoscience and Remote Sensing Letters*, *14*(1), 48–51. https://doi.org/10.1109/LGRS.2016.2625302

[16] Li, T., Zhao, X., Zhang, J., Wang, S., & Tan, Z. (2018). A new compensation method for magnetic field distortions based on a 3-D Helmholtz coil. *Measurement Science and Technology*, *30*(1), 015006. https://doi.org/10.1088/1361-6501/aaef04

[17] Sasayama, T., Gotoh, Y., & Enpuku, K. (2018). Improving tip position-estimation performance of gastric tube by compensating geomagnetic field with offset coils. *IEEE Transactions on Magnetics*, *54*(11), 1–5. https://doi.org/10.1109/TMAG.2018.2846267

[18] Hou, R. F., Zhang, Z. G., Dai, L., Gong, W. J., & Lin, A. L. (2014). The Calibration method of Helmholtz coils for the permanent Magnet. *In Advanced Materials Research* (Vol. 1006, pp. 849–852). Trans Tech Publications Ltd. https://doi.org/10.4028/www.scientific.net/AMR.1006-1007.849

[19] Bamer, F., & Bucher, C. (2012). Application of the proper orthogonal decomposition for linear and non-linear structures under transient excitations. *Acta Mechanica*, *223*, 2549–2563. https://doi.org/10.1007/s00707-012-0726-9

[20] Danlos, A., Ravelet, F., Coutier-Delgosha, O., & Bakir, F. (2014). Cavitation regime detection through Proper Orthogonal Decomposition: Dynamics analysis of the sheet cavity on a grooved convergent–divergent nozzle. *International Journal of Heat and Fluid Flow*, *47*, 9–20. https://doi.org/10.1016/j.ijheatfluidflow.2014.02.001

[21] Penenko, V., & Tsvetova, E. (2008). Orthogonal decomposition methods for inclusion of climatic data into environmental studies. *Ecological Modelling*, *217*(3–4), 279–291. https://doi.org/10.1016/j.ecolmodel.2008.06.004

[22] Yu, G., Yu, B., Han, D., & Wang, L. (2013). Unsteady-state thermal calculation of buried oil pipeline using a proper orthogonal decomposition reduced-order model. *Applied Thermal Engineering*, *51*(1–2), 177–189. https://doi.org/10.1016/j.applthermaleng.2012.09.005

[23] Ly, H. V., & Tran, H. T. (2001). Modeling and control of physical processes using proper orthogonal decomposition. *Mathematical and Computer modelling*, *33*(1–3), 223–236. https://doi.org/10.1016/S0895-7177(00)00240-5

Kuankuan Zhang has been pursuing a Ph.D. degree at the University of Science and Technology Beijing (USTB) since 2017. His main research interests include metrology and service performance evaluation of magnetic materials.

Mingxing Cao received her MSc. degree from Beijing University of Technology (BJUT), China in 2020. Starting from 2023, she has held assistant engineering positions in the National Institute of Metrology in China where she is involved in developing measurement for magnetic materials.

Jian He received his B.Sc. degree from Northestern University, China in 2002 and the M.Sc. degree from the University of Science and Technology Beijing (USTB) in 2005. After that, he joined the National Institute of Metrology, China. His current research interests include magnetic materials measurement and standardization technology. He is a member of IEC TC68 working group 5.

Wenjie Gong was born in Hubei, China, in 1984. He received the B.E. degree from Central South University, Hunan, China. Then, he received the Ph.D. degree in materials science and engineering with a specialization in magnetic materials from the Institute of Metal Research, Chinese Academy of Sciences, Liaoning, in 2013. Next, he joined magnetic measurement laboratories at the National Institute of Metrology (NIM), China, where he worked on magnetic measurement of electrical steel and soft magnetic materials. He is currently an associate researcher in NIM and his research interests include the development of measuring and calibration methods for magnetic materials.

Metrol. Meas. Syst., Vol. 30 (2023), No. 3, pp. 549–561
DOI: 10.24425/mms.2023.146415

Yunhua Huang obtained the Ph.D. in materials physics and chemistry from the University of Science and Technology Beijing (USTB), China in 2006. He is currently Professor of the Institution for Advanced Materials and Technology, and National Materials Corrosion and Protection Data Center at USTB. He has authored or coauthored 4 books and book chapters, over 200 journal and conference publications. He has led 6 NSFC and other national projects, and has received over 10 academic awards. His current research focuses on metals corrosion and protection.